Nondestructive Evaluation Using a High-T_C SQUID Microscope

Michael I. Faley, E. A. Kostyurina, P. Diehle, Ulrich Poppe, A. Kovacs, Yuri V. Maslennikov, Valery P. Koshelets, and Rafal E. Dunin-Borkowski

***Abstract*—We report the application of a scanning high-T_c SQUID (superconducting quantum interference device) microscope with a ferromagnetic flux guide for the nondestructive evaluation of weld seams and wear tracks and scars on austenitic stainless steel plates as well as measurement of magnetic stray fields distribution above patterned by electron lithography 30-nm-thick cobalt films. A soft magnetic amorphous Vitrovac foil was used to guide the flux from the samples, which were held at room temperature, to the liquid-nitrogen-cooled SQUID-sensor and back. The flux guide passes through a hole in the 1 mm × 2.5 mm pick-up loop of the high-T_c SQUID sensor, thereby providing improved coupling of the magnetic flux from the object to the SQUID. In order to avoid the influence of the SQUID biasing the magnetic field on the object under investigation, a modulation and feedback coil was coupled to the pick-up loop of the SQUID directly and beyond the ferromagnetic flux guide. Such decoupling of feedback coil from soft magnetic flux antenna ensures that the high-T_c SQUID microscope does not disturb the sample magnetization during image recording. The SQUID microscope can be used to measure the spatial distribution of the *z*-component of the stray field above a specimen without mechanical contact to it.**

***Index Terms*—Magnetic analysis, magnetic sensors, nondestructive testing, scanning probe microscopy, SQUIDs.**

I. Introduction

SPATIAL imaging of magnetic fields generated by room temperature objects is a powerful technique for evaluation of wear defects in industrial materials and magnetic state of spintronic devices. Different scanning methods are used for testing of objects of different size: from large ones like detection of tendon ruptures in prestressed highway concrete bridges by high-T_c superconducting quantum interference devices (SQUIDs) [1] to magnetic microscopy of nanostructures with approximately 10 nm spatial resolution using nitrogen vacancies in diamond [2], electron holography [3] and magnetic force microscopy [4]. For object dimensions between 10 and 10^4 μm Hall probe microscopy [5] and magneto-optical sensors [6] are currently used in most cases. Different scanning SQUID microscopes (SSM) cover all these ranges of object dimensions and have the best magnetic field sensitivities. In the case of nanosized low-T_c SQUIDs and cold investigated object unprecedented spin sensitivity approximately $0.38\,\mu_B/\sqrt{\text{Hz}}$, where μ_B is Bohr magneton, was achieved at 4.2 K [7]. SSM is a powerful tool for fundamental and applied research (see for example [8] and [9]).

The spatial resolution of SSM is usually limited by the sensor area or by the distance between sensor and sample. For SSM with low-T_c SQUID and cold investigated object the flux sensing area of the SQUID should be small. For investigation of room temperature samples spatial resolution of SSM is limited by standoff distance to the investigated objects as the cold SQUID sensor has to be thermally isolated. SSMs with high-T_c SQUIDs have advantage of a typically smaller standoff distance to the investigated objects at room temperature than SSMs with low-T_c SQUIDs. SSMs with high-T_c SQUIDs can be used for investigation of room temperature samples, for example, for localization of buried defects in semiconductor circuits or for characterization of magneto-electronic devices [9, 10, and 11]. For SSM, which use bare high-T_c SQUID as a sensor, "sample-to-sensor" separation between 15 and 50 μm were achieved [12] leading to the spatial resolutions of approximately 50 μm.

To overcome this drawback of a large standoff distance, different versions of scanning SQUID microscopes where high-T_c SQUIDs were combined with a soft ferromagnetic tip, which served as a magnetic flux antenna, have been investigated [13, 14, 15 and 16]. The decay of the flux transported from the sample at the sharp end of the tip to the SQUID at the other end of the tip is substantial in the designs represented in [13] and [14] as no low loss return of magnetic flux to the sample is provided. We have developed a SSM in which a soft magnetic antenna guides the magnetic flux from room temperature object to high-T_c dc-SQUID; passes a hole in its pickup loop and returns the magnetic flux back to the object [15], [16]. Smaller magnetic reluctance of the way through the pick-up loop of the SQUID in such magnetic circuit improves magnetic coupling between the object and the SQUID. Here, we describe a modification of magnetic circuit in such SSM and tested it using measurements of magnetic stray fields of different room temperature objects.

II. Experimental

The high-T_c DC SQUIDs were made from 200 nm thick superconducting $YBa_2Cu_3O_{7-x}$ (YBCO) films deposited by high-oxygen-pressure sputtering technique [17] on 24°

Manuscript received September 7, 2016; accepted October 23, 2016. Date of publication November 21, 2016; date of current version December 16, 2016. This work was supported in part by the Russian Scientific Foundation under Project 15-19-00206. *(Corresponding author: Michael I. Faley.)*

M. I. Faley, P. Diehle, U. Poppe, A. Kovacs, and R. E. Dunin-Borkowski are with the PGI-5 Forschungszentrum Jülich GmbH, Jülich 52428, Germany (e-mail: m.faley@fz-juelich.de; p.diehle@fz-juelich.de; U.Poppe@fz-juelich.de; a.kovacs@fz-juelich.de; rafaldb@gmail.com).

E. A. Kostyurina is with the Moscow Institute of Physics and Technology (State University), Dolgoprudny, Moscow Region, 141700, Russia and also with the Kotel'nikov Institute of Radio Engineering and Electronics, Moscow 125009, Russia (e-mail: kostyurina.katya@gmail.com).

Y. V. Maslennikov and V. P. Koshelets are with the Kotel'nikov Institute of Radio Engineering and Electronics RAS, Moscow 125009, Russia (e-mail: cryoton@inbox.ru; valery@hitech.cplire.ru).

Color versions of one or more of the figures in this paper are available online at http://ieeexplore.ieee.org.

Digital Object Identifier 10.1109/TASC.2016.2631419

bicrystal $SrTiO_3$ substrates. The SQUID has a 1 μm wide Josephson junctions and 100 μm $\times$ 10 μm SQUID loop, which is directly coupled to 1 mm $\times$ 2.5 mm pick-up loop. A 1.5 mm $\times$ 0.3 mm hole was made inside the pick-up loop of the SQUID by ultra-sonic cutting [15]. The SQUID and the hole were produced approximately 14 years ago. During this time period, the critical current of the SQUID has increased from 150 μA to 170 μA at 77 K, but the white noise of approximately 500 fT/$\sqrt{}$Hz at 77 K remained unaltered.

A copper coil, which is used both for modulation and feedback, was wound around a bundle of ferromagnetic wires leading magnetic flux to the hole un the pick-up loop of the SQUID, see Fig. 1(a). For the flux guidance we have used an amorphous soft magnetic 25 μm thick foil made from a Fe-Mo-Co-B-Si -alloy (Vitrovac 6025).[1] Double-layer of such foil was led through the same hole in the pick-up loop and returned back sidewards from the SQUID. The construction, shown in the Fig. 1(a) is fixed on a cooled by liquid nitrogen sapphire rod in the vacuum part of a fiberglass cryostat. The SQUID, modulation coil and the Vitrovac antenna were fixed relative to each other by vacuum grease. The Vitrovac tip, which catches magnetic flux from the investigated object, and the Vitrovac foil for return of magnetic flux back to the object are vacuum sealed by epoxy in the cryostat window at room temperature and connected loosely to their cooled counterparts as it is shown in the Fig. 1(b).

The antenna was cut from the Vitrovac foil normal to its rolling direction in order to achieve a continuous rotation of domains during magnetization. The highly permeable (μ_r about 10^5) Vitrovac foil shows a very small hysteresis (coercivity $<$ 10 A/ m $\cong$ 0.13 Oe and negligible magnetostriction $<0.2 \times 10^{-6}$) and led to only a small amount of additional noise to the SQUID. The Vitrovac tip was sharpened by a 0.3 μm diamond polishing sheets and has at the end a curvature radius of approximately 200 nm. SEM image of the Vitrovac tip used in the present study is shown in the Fig. 1(c). The antenna and the SQUID were shielded by an additional Vitrovac foil except the region near a 100 μm round hole in the shielding, where the end of the tip was placed. In this case mainly the magnetic flux produced in the sample region near the end of the tip is led to the SQUID sensor. The SQUID was fixed from the outer cryostat wall at distance approximately 2 mm. The distance from the SQUID to the sharp end of the sensing tip was about 3 mm. The operation temperature SQUID during the measurements was about 78 K.

The lower part of the cryostat containing the SQUID and the flux guide was additionally surrounded by two μ- metal layers to shield them by a factor of about 50 from external magnetic disturbances, which originate mainly from motors of the scanning stage and 50 Hz line frequency. This double shield also deflected constant magnetic fields, which are dominated by earth magnetic field, so that the magnetic antenna was operating in the linear region of the magnetization as a function of field where the magnetization is reversible.

The damping of magnetic signals by induction of eddy currents in the highly resistive and 25 μm thick Vitrovac foil in the frequency range below 10 kHz was negligible. The amorphous Vitrovac foil has also relatively low thermal conductivity so that no significant heat was leaked to the SQUID and the sapphire rod in the cold part of the cryostat. In the cryostat contains about 0.8 l of liquid nitrogen and requires refilling after approximately 2 days of measurements.

The SSM measures the component of magnetic stray field directed perpendicular to the sample surface. The sample is fixed on a non-magnetic plastic plate including a non-magnetic levelling stage compensating for small tilts of the sample holder. The

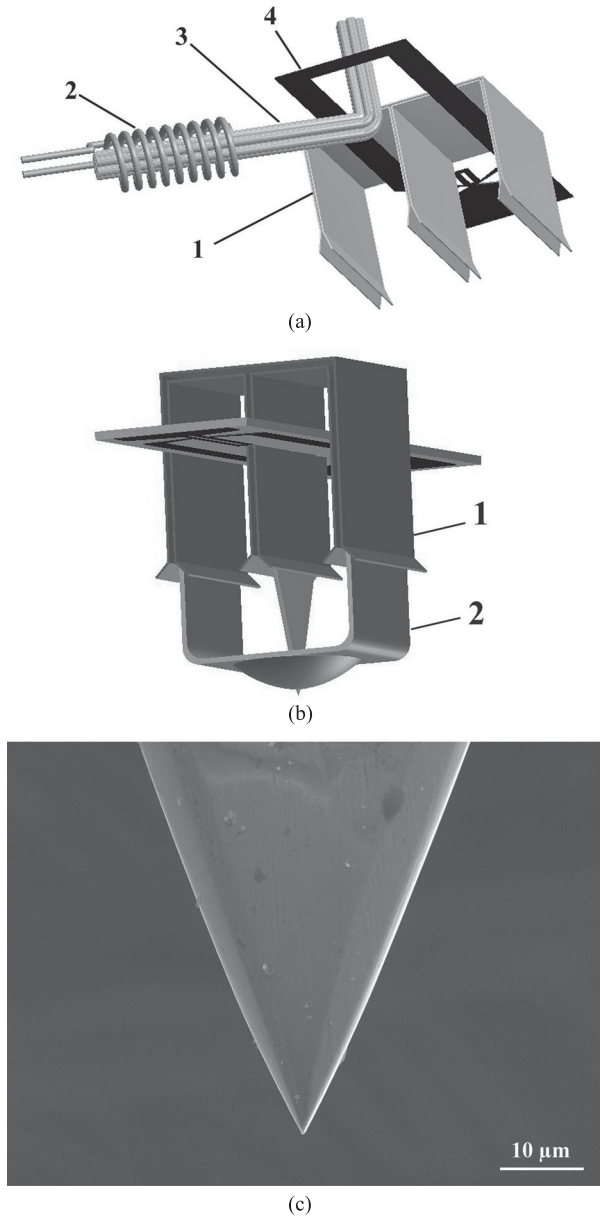

Fig. 1. (a) Sketch of a DC SQUID assembled with the low temperature part of magnetic flux antenna (1) and a coil (2) wounded around a bunch of ferromagnetic wires (3) leading flux modulation and feedback signals to pick up loop (4) of the SQUID, (b) sketch of SQUID with magnetic flux antenna (1) assembled with its room temperature counterpart (2), and (c) SEM image of the tip of the Vitrovac foil, which is used in the present study. The tip has at the end a curvature radius of approximately 200 nm.

[1] Vitrovac 6025 is a product of Vacuumschmelze GmbH, Hanau, Germany.

levelling stage provides nearly constant distance of typically a few μm between flat sample surface and the end of the antenna tip during the scanning process. The sample was moved by a precision x-y scanning stage and a z-translation stage driven by micro-step stepper motors providing a positional resolution better than 1 μm over a large scan range of more than 15 cm. Two high magnification optical telescopes were used for initial positioning of the sample under the tip and levelling of the sample surface parallel to the x-y scanning plane. The stepper motors were magnetically shielded by 1 mm thick Cryoperm caps. Distance between the motors and the sensing tip was more than 40 cm. The scan area, scanning speed, the data acquisition and image processing were controlled by a computer. The SQUID was operated in a flux-locked loop mode using a commercial ac-bias electronic [18]. The output voltage of the electronics is proportional to the flux guided from the tip of the Vitrovac antenna through the pick-up loop of the SQUID. The signal from the SQUID electronics was additionally filtered by a 50 Hz notch filter and a 12-order Butterworth 10 Hz-low-pass filter, which suppressed 50 Hz line frequency and higher harmonics. Magnetic field sensitivity of the SSM was calibrated using an 80 μm round current loop similar to the procedure described in the previous publication [15]. The investigated samples were not intentionally magnetized.

III. Results

The functionality of the instrument was tested by measurements on different test objects: banknotes, weld seams and wear tracks on stainless steel plates, and thin film Co-pattern on SiN membrane. These examples demonstrate non-destructive and non-contact operation of the SQUID microscope at different levels of the magnetic signals, morphology of the surface and the required spatial resolution.

For the sake of comparison, we have performed a "traditional" [19], [20] measurement of magnetic field distribution over a US 1 $ bill. Magnetic ink used for printing of banknotes contains small amount of nanoparticles of magnetite - black iron oxide Fe_3O_4 - that exhibit a remnant magnetization. The result of our measurements is shown in the Fig. 2.

The amplitude of magnetic stray fields was about 6 μT and signal-to-noise ratio was above 100, which confirms the measured sensitivity of the system at 1 Hz (see Fig. 2 in [15]) and which is comparable with other SQUID microscopes. The 100-μm spatial resolution of these measurements was limited by the 100 μm distance between the tip and the bill surface. Multiple reproducible tests confirm also negligible opposite influence of the SQUID feedback coil and the magnetic flux antenna on the magnetization state of magnetic particles in the ink. The magnetic fields are so strong in this example that for the practical visualization of magnetic structures on currencies with similar spatial resolution is it easier to use Faraday effect, which is implemented for example in a magneto-optical system CMOS-MagView [21]. But the magnetic properties of the bills tend to degrade with age. In such case the use of SQUID microscope system can be justified because the conventional magnetic-ink testers tend to give many false positives for counterfeits for testing of old and heavily used banknotes.

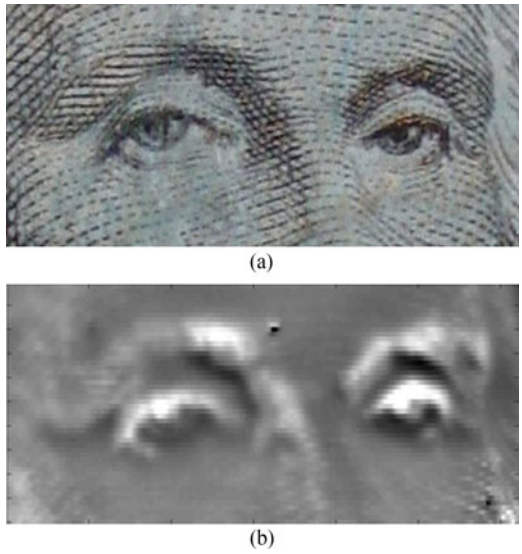

Fig. 2. (a) A photograph of a part of a US $1 bill used for the performance test and (b) a grey-scale image represents the magnetic field distribution over the same area. The grey-scale value represents the magnetic field strength, which ranges from -3μT (black) to 3 μT (white). Scan area: 12 mm $\times$ 5 mm.

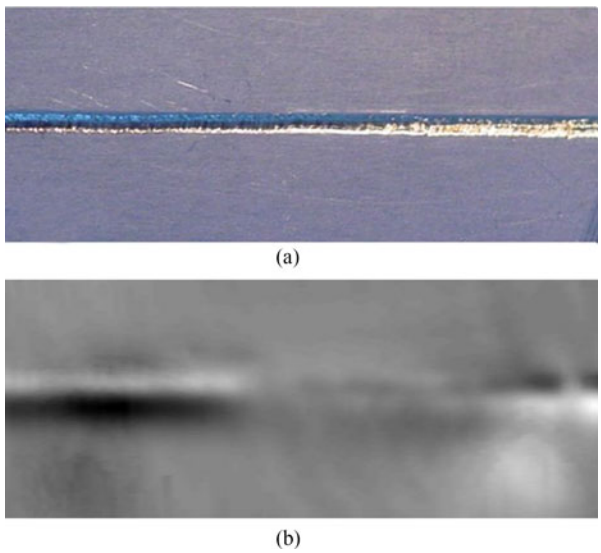

Fig. 3. (a) A photograph of a part of a weld seam made by laser welding and (b) a grey-scale image of the magnetic field distribution over this area. The range of the grey-scale values is approximately from -100 nT (black) to 100 nT (white). Scan area: 20 mm $\times$ 8 mm.

Next two experiments are related to non-destructive evaluation of magnetic features in stainless steel samples caused by welding and wearout. Metastable austenitic corrosion resisting steel X5CrNi18-10 German grade 1.4301 (AISI 304) is not magnetic and often used for cryogenic applications because even at low temperatures it retains its strength at high loads. Heat treatment or wear of austenitic stainless steels partially transform austenite to martensite which is ferromagnetic and brittle and this can lead to dysfunction of devices.

Fig. 3 shows the optical and magnetic images of a weld seam made by a laser welding. The steel 1.4301 is very suitable for laser beam welding because for small welding groove width and thin products the use of filler metals is not necessary. Observed magnetic signal along the weld seam made between 1

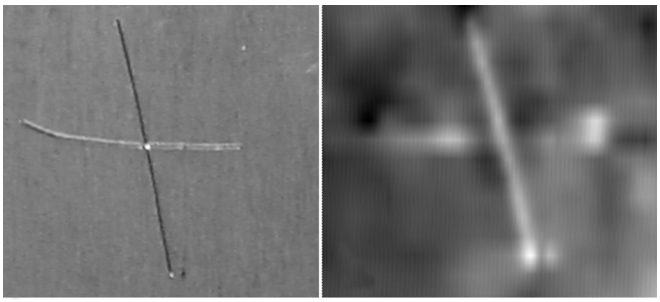

Fig. 4. (a) A photograph of a part of a stainless steel plate including scratches made by a diamond; (b) magnetic field distribution measured over the same area and shown in grey-scale range from −100 to 100 nT. Scan area: 5 mm × 5 mm.

mm thick steel plates (see Fig. 3(b)) is relatively weak and comparable with the amplitude of magnetic signals originated from the welded plates. For comparison, magnetic field above seams of wolfram-inert-gas-welding (WIG-welding) of the same steel plates is more than 10 times stronger.

During the welding of this steel, structural changes occur. Consequently the permeability of the metal in the weld, and the surrounding heat affected zone, can be significantly higher than in the original parent material. Difference in magnetic signals between WEG- and laser weldings can be explained by a much more rapid cooling from high temperatures preventing transformation of austenite phase to $\acute{\alpha}$-martensite in the case of laser welding. Magnetic field measurements by the SQUID microscope have not changed magnetization of these samples.

Similar amplitude of stray fields was observed above scratches made at room temperature by a diamond tip on the surface of the 1.4301 stainless steel plates. The photograph of the scratches and the measurement results are shown in Figs. 4(a) and 4(b), respectively. Cold working and tribological stressing of austenitic stainless steels can partially transform the nonmagnetic austenite on the surface to ferromagnetic $\acute{\alpha}$-martensite via plastic deformation [22]. Sensitivity of the SQUID microscope is sufficient to detect magnetic signal from a single wear track, while in standard tribological experiments more than 500 cycles are usually performed [22]. The described above measurements were performed at scan speed 200 μm/sec at about 100 μm distance between the tip of magnetic antenna and sample surface.

The SQUID microscope can be used to investigate magnetic coupling through barriers or the influence of pinholes in magnetic tunnel junctions or other spintronics devices. We have observed different magnetic domain structure distributions in the thin iron films separated by from 0.6 nm up to 1.6 nm thick $(SiGe)_n$-barrier [23]. We have also observed dependent from magnetization different magnetic stray field distributions in $Co/Al_2O_3/Co$-tunnel junction of tunneling magneto-resistive devices. Such thin film samples with static magnetic moments are used for recording media and for magneto-electronic devices.

Another challenging experiment is intended to compare the results obtained from the same specimens using the SQUID microscope and using off-axis electron holography and Lorentz imaging techniques in the transmission electron microscope. A

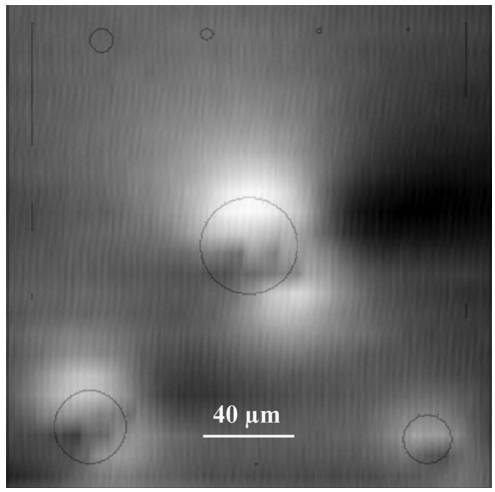

Fig. 5. Magnetic field distribution over the Co-pattern on SiN membrane shown in grey-scale in the range from −10 nT to 10 nT. Contours of the investigated Co-pattern are added to the image. Signals and magnetic domain structure of 40, 30, and 20 μm dots are visible.

pattern of 30 nm thick Co films was fabricated by electron beam lithography on 50 nm thick SiN membrane and protected from oxidation by an Al layer on top of the Co pattern. The measurements were performed in the frequency bandwidth (0.03–1) Hz with speed 8 μm/sec at about 10 μm distance between the tip of magnetic antenna and the membrane. Results of the measurements are represented in Fig. 5. Signal-to-noise ratio for the 40 μm Co disc is about 30 while the magnetic signals originated from the structures smaller than 10 μm are below noise level. There are also 0.3 μm wide bar Co structures on the membrane, but their magnetic signals were also below noise level of the SSM.

The observed dependence of the magnetic signal on the size of the circular thin-film Co structures is strongly nonlinear. This is because the magnetic moment of the structures is rather dependent on the volume of magnetic material than on its linear size. Additionally, rapid decrease of the signal is expected when the size of the structures becomes comparable with the size of the tip of the magnetic antenna or with the distance between the tip and the sample. Current spatial resolution of the SSM is still not sufficient for direct comparison with off-axis electron holography because the latter has the current field-of-view of smaller than 3 μm. The results of the measurements of magnetic fields originated from the Co pattern using off-axis electron holography and Lorentz imaging techniques in the transmission electron microscope will be published elsewhere [24].

IV. Conclusion

New tests were performed with high-T_c SSM with a flux guide antenna made from an extremely soft magnetic amorphous Vitrovac foil. This SSM does not disturb the sample magnetization during image recording and operates in non-contact mode. Non-destructive evaluations of magnetic features in weld seams and wear tracks and scars on austenitic stainless steel plates as well as measurement of magnetic stray field distribution above patterned by electron lithography 30 nm thick cobalt films on 50 nm thick SiN membrane were performed.

REFERENCES

[1] H.-J. Krause *et al.*, "SQUID array for magnetic inspection of prestressed concrete bridges," *Physica C: Supercond.*, vol. 368, no. 1–4, pp. 91–95, 2002.

[2] L. Rondin, J.-P. Tetienne, T. Hingant, J.-F. Roch, P. Maletinsky, and V. Jacques, "Magnetometry with nitrogen-vacancy defects in diamond," *Rep. Prog. Phys.*, vol. 77, 2014, Art. no. 056503.

[3] R. E. Dunin-Borkowski, M. R. McCartney, R. B. Frankel, D. A. Bazylinski, M. Pósfai, and P. R. Buseck, "Magnetic microstructure of magnetotactic bacteria by electron holography," *Science*, vol. 282, pp. 1868–1870, 1998.

[4] I. V. Yaminsky and A. M. Tishin, "Magnetic force microscopy," *Russian Chem. Rev.*, vol. 68, no. 3, pp. 165–170, 1999.

[5] A. M. Chang *et al.*, "Scanning hall probe microscopy," *Appl. Phys. Lett.*, vol. 61, 1992, Art. no. 1974.

[6] M. Koschny and M. Lindner, "Magneto-optical sensors: accurately analyze magnetic field distribution of magnetic materials," *Adv. Mater. Processes*, vol. 170, no. 2, pp. 13–16, 2012.

[7] D. Vasyukov *et al.*, "A scanning superconducting quantum interference device with single electron spin sensitivity," *Nature Nanotechnol.*, vol. 8, pp. 639–644, 2013.

[8] J. R. Kirtley and J. P. Wikswo, "Scanning SQUID microscopy," *Annu. Rev. Mater. Sci.*, vol. 29, pp. 117–148, 1999.

[9] D. Vallett, "Magnetic current imaging revisited," *ASM Int.*, vol. 4, pp. 26–34, 2014.

[10] M. Mück, "SQUIDs: microscopes and nondestructive evaluation," *Phys. Status Sol. (C)*, vol. 2, no. 5, pp. 1510–1523, 2005.

[11] V. V. Talanov, N. M Lettsome, Jr., V. Borzenets, N. Gagliolo, A. B. Cawthorne, and A. Orozco, "A scanning SQUID microscope with 200 MHz bandwidth," *Supercond. Sci. Technol.*, vol. 27, 2014, Art. no. 044032.

[12] T. S. Lee, Y. R. Chemla, E. Dantsker, and J. Clarke, "High-T_c SQUID microscope for room temperature samples," *IEEE Trans. Appl. Supercond.*, vol. 7, no. 2, pp. 3147–3150, Jun. 1997.

[13] S. Tanaka, K. Matsuda, O. Yamazaki, M. Natsume, H. Ota, and T. Mizoguchi, "Properties of high-T_c superconducting quantum interference device microscope with high μ-metal needle," *Jpn. J. Appl. Phys.*, vol. 40, pp. L431–L433, 2001.

[14] S. A. Gudoshnikov *et al.*, "Flux guide for high-T_c SQUID microscope with high spatial resolution," *Physica C*, vol. 372–376, pp. 271–273, 2002.

[15] U. Poppe *et al.*, "HTS dc-SQUID microscope with soft-magnetic flux guide," *Supercond. Sci. Technol.*, vol. 17, pp. S191–S195, 2004.

[16] M. I. Faley *et al.*, "Magnetic flow sensor comprising a magnetic field conductor and a hole diaphragm," US Patent 7221156 (B2), May 22, 2007.

[17] U. Poppe *et al.*, "Low-resistivity epitaxial $YBa_2Cu_3O_{7-x}$ thin films with improved microstructure and reduced microwave losses," *J. Appl. Phys.*, vol. 71, pp. 5572–5578, 1992.

[18] Cryoton Co. Ltd., Lesnaja str., 4B, Moscow, Troitsk 142190, Russia.

[19] F. C. Wellstood, A. Mathai, D. Song, and R. C. Black, "Method and apparatus for imaging microscopic spatial variations in small currents and magnetic fields," US Patent US5491411, Feb. 13, 1996.

[20] M. I. Faley *et al.*, "HTS dc-SQUID micro-susceptometer for room temperature objects," *Supercond. Sci. Technol.*, vol. 17, pp. S324–S327, 2004.

[21] Matesy GmbH—Magnetic Technologies and Systems, Otto-Schott-Straße 13, 07745 Jena, Germany.

[22] K. Assmus, W. Hübner, A. Pyzalla, and H. Pinto, "Structure transformations in CrNi steels under tribological stressing at low temperatures," *Tribotest*, vol. 12, pp. 149–159, 2006.

[23] R. R. Gareev, M. Weides, R. Schreiber, and U. Poppe, "Resonant tunneling magnetoresistance in antiferromagnetically coupled Fe-based structures with multilayered Si/Ge spacers," *Appl. Phys. Lett.*, vol. 88, 2006, Art. no. 172105.

[24] P. Diehle *et al.*, to be published.